

One-pot Synthesis of PtSn Bimetallic Composites and Their Application as Highly Active Catalysts for Ethanol Electrooxidation

Yue Feng,^[a] Caiqin Wang,^[a] Duan Bin,^[a] Chunyang Zhai,^[a] Fangfang Ren,^{*,[b]} Ping Yang,^[a] and Yukou Du^{*,[a]}

PtSn nanoparticles with different molar ratio are fabricated by chemical reduction to form a relatively efficient catalyst for ethanol electrooxidation in an alkaline solution of KOH (1.0 M) containing C₂H₅OH (1.0 M). The surface composition and structure of the as-prepared catalysts are characterized by using scanning electron microscopy (SEM), transmission electron microscopy (TEM), X-ray diffraction (XRD), X-ray photoelectron spectroscopy (XPS), and energy dispersive X-ray spectroscopy (EDX). Cyclic voltammogram (CV) and chronoamperometric

(CA) measurements are used to evaluate the electrochemical activity and stability of the as-prepared catalysts. As the content of Sn in the catalysts changed, the catalysts showed different catalytic activity. The results indicate that the moderate addition of Sn can enhance the catalytic activity of Pt catalyst, and Pt₃Sn₁ displays the highest catalytic activity and stability among the as-synthesized PtSn nanoparticles during the electrooxidation of ethanol.

Introduction

With increasing demands for energy and limitations surrounding fossil fuels, there is great interest in developing direct fuel cells. It is known that liquid fuels can be stored easily in comparison with gas fuels such as H₂^[1] and CH₄.^[2] Methanol and ethanol are two such electroactive fuels. Methanol can be nearly completely electrooxidized to the final product of CO₂ because of its simple molecular structure. On the other hand, ethanol is less toxic,^[3] less corrosive, and easily stored compared with methanol, and it can be produced in a sustainable way. As a result, researchers pay more attention to ethanol oxidation because of its potential application in direct ethanol fuel cells.

An efficient catalyst for ethanol electrooxidation should possess the following attributes: 1) the ability to break C–C bonds of the ethanol molecule under mild condition and 2) high tolerance to immediate species generated over the surface of the catalysts during alcohol electrooxidation.^[4] It is known that highly dispersed Pt and Pt-based nanoparticles have been widely used as catalysts for ethanol electrooxidation, because they possess particular properties.^[5,6,7] Platinum-based catalysts, including Pt, Pt-based alloys, and Pt modified with other

metal/non-metal materials have been investigated over the past few decades.^[8,9] The catalytic activity of pure Pt for ethanol electrooxidation is limited because Pt will be easily poisoned by intermediate species such as CO during the electrooxidation process.^[10,11] Moreover, Pt is extremely expensive, so it is necessary to decrease the use of Pt and improve its applicability.^[12] The addition of Au, Ru, or Sn has proved to be an effective strategy.^[13] Among these elements, Sn is low-cost and widely available, and is thus preferred for the prepare PtSn binary catalysts for ethanol electrooxidation.^[14] Many researchers have investigated the role which Sn plays in enhancing the catalytic activity.^[15,16,17] The Sn changes the electronic structure of Pt and as a result decreases CO adsorption on the surface of Pt.^[17]

A variety of methods have been used to prepare PtSn catalysts. The polyol method has been proposed as a suitable approach in which the PtSn/C (Pt/Sn = 1:1) electrocatalysts were prepared.^[4,18–20] Also, pulse microwave deposition is a facile approach to fabricate PtSn catalysts onto graphene nanosheets (GNs) within a short time.^[21] In addition, simple chemical methods have been used to preparation PtSn catalysts,^[22,23] which show good catalytic performances towards ethanol oxidation.

Herein, catalysts composed of PtSn with different molar ratio such as Pt₁Sn₂, Pt₁Sn₁, Pt₂Sn₁, Pt₃Sn₁, and Pt₅Sn₁ were synthesized by a one-pot chemical reduction method, using solutions of sodium borohydride (to reduce chloroplatinic acid) and stannous chloride. The catalytic activity and stability of as-prepared catalysts were evaluated in an alkaline medium. The results indicate that the addition of Sn can obviously affect the catalytic activity of Pt catalysts, where Pt₃Sn₁ displayed the highest catalytic activity and stability during the electrooxidation of ethanol.

[a] Y. Feng, C. Wang, D. Bin, C. Zhai, Prof. P. Yang, Prof. Y. Du
College of Chemistry, Chemical Engineering and Materials Science
Soochow University
Suzhou 215123 (P. R. China)
E-mail: duyk@suda.edu.cn

[b] Dr. F. Ren
Analysis and Testing Center
Yancheng Teachers University
Yancheng 224051 (P. R. China)
E-mail: fangfang7916@163.com

Supporting information for this article is available on the WWW under <http://dx.doi.org/10.1002/cplu.201500315>.

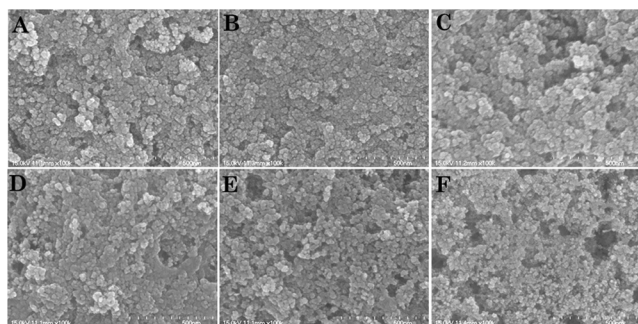


Figure 1. SEM images of Pt₁Sn₁ (A), Pt₁Sn₂ (B), Pt₂Sn₁ (C), Pt₃Sn₁ (D), Pt₅Sn₁ (E), and Pt (F).

Results and Discussion

Characterization of the as-prepared PtSn catalysts

The SEM images of all samples of catalysts are shown in Figure 1. The nanoparticles of PtSn and Pt catalysts prepared by the chemical reduction method display a porous structure. Although the PtSn catalysts have different proportions of Pt and Sn, there is no apparent difference in the particle morphology and the structure among all the catalysts.^[10,24] It is possibly because that all these catalysts were prepared by the same methods.

Meanwhile, EDX analysis was performed to analyze the surface composition of all as-prepared catalysts^[25,26] (Figure 2). The molar ratio of Pt to Sn for Pt₁Sn₂, Pt₁Sn₁, Pt₂Sn₁, Pt₃Sn₁, and Pt₅Sn₁ catalysts shown in Table 1. These molar ratios were measured to be 0.49, 1.02, 1.75, 3.13, and 4.95, respectively, which are consistent with the molar ratio of Pt and Sn precursors before reduction. This outcome reveals that the as-prepared catalysts have molar ratios consistent with the precursors but with some variation in composition, thus the chemical reduction method applied in this study is suitable and reliable.

It is well-known that the formation of PtSn alloy is extremely easy.^[27–29] As already mentioned in the introduction, tin-alloying effects on the electronic structure of PtSn surfaces can enhance the catalytic activity for ethanol electrooxidation.^[30] In addition, Sn can be easily oxidized in air without the need for an inert atmosphere such as argon or nitrogen.^[31,32] The crys-

Table 1. The experimental EDX results for the PtSn catalysts.

	Pt ₁ Sn ₂	Pt ₁ Sn ₁	Pt ₂ Sn ₁	Pt ₃ Sn ₁	Pt ₅ Sn ₁
predicted molar ratio of Pt/Sn	1:2	1:1	2:1	3:1	5:1
experimental molar ratio of Pt/Sn	0.98:2	1.02:1	1.75:1	3.13:1	4.95:1

tal structure of these PtSn catalysts was determined using X-ray diffraction.^[33] In Figure 3, the signals at around 39.6°, 46.2°, 67.3°, and 81.5° are attributed to the diffraction peaks of face-centered cubic planes of Pt (111), Pt (200), Pt (220), and Pt (311).^[2] In the case of PtSn catalysts, the corresponding diffraction peaks at about 26° and 34° are assigned to SnO₂ (110) and (101) planes, thus indicating that Sn has been successfully introduced into the Pt catalysts in the form of SnO₂.^[34,35] According to prior reports^[27–29,31,32] and results of XRD analysis, we can reasonably assume that the PtSn alloy is first formed and tin is gradually oxidized into tin oxide upon storage.

X-ray photoelectron spectroscopy was used to identify the Sn composition (Figure 4). Table 2 presents the binding energies of elemental Pt and Sn in various as-obtained catalysts determined from their XPS spectra and match those values already reported.^[36–38] In the entire Pt spectra, the 4f^{7/2} signal at around 71.50 eV for all catalysts are assigned to zero-valent Pt. The binding energies of Sn are slightly higher than the reference data,^[36–38] owing to interactions between Sn and Pt resulting from a higher Sn content or small cluster-size effects.^[37]

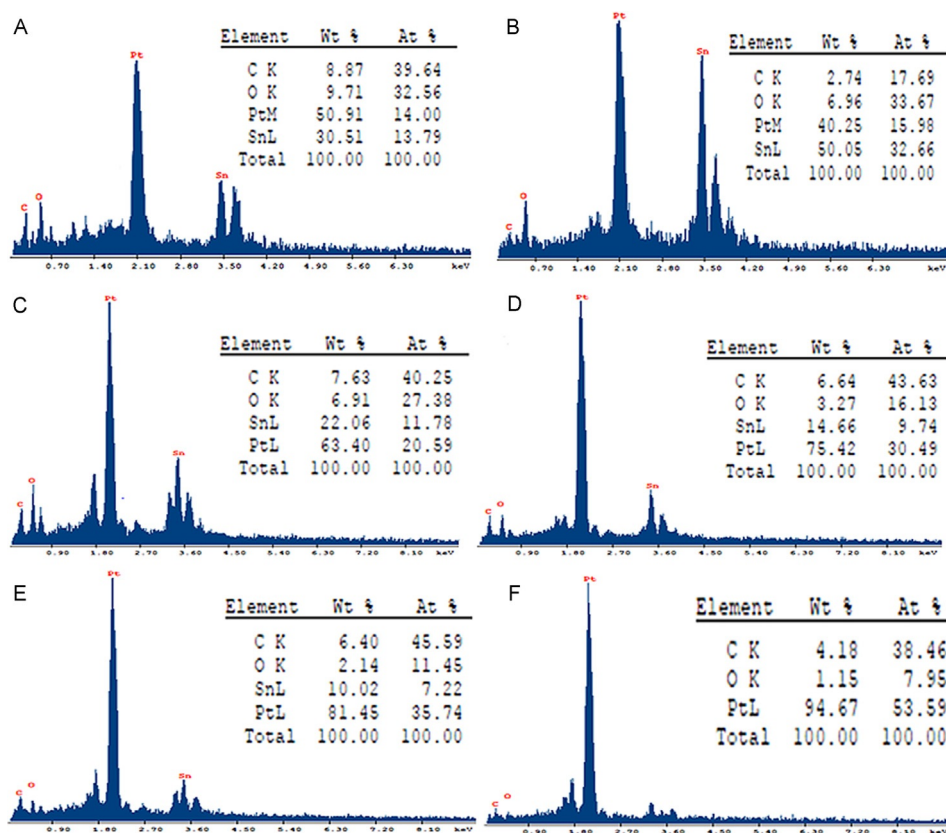


Figure 2. EDX image for Pt₁Sn₁ (A), Pt₁Sn₂ (B), Pt₂Sn₁ (C), Pt₃Sn₁ (D), Pt₅Sn₁ (E), and Pt (F).

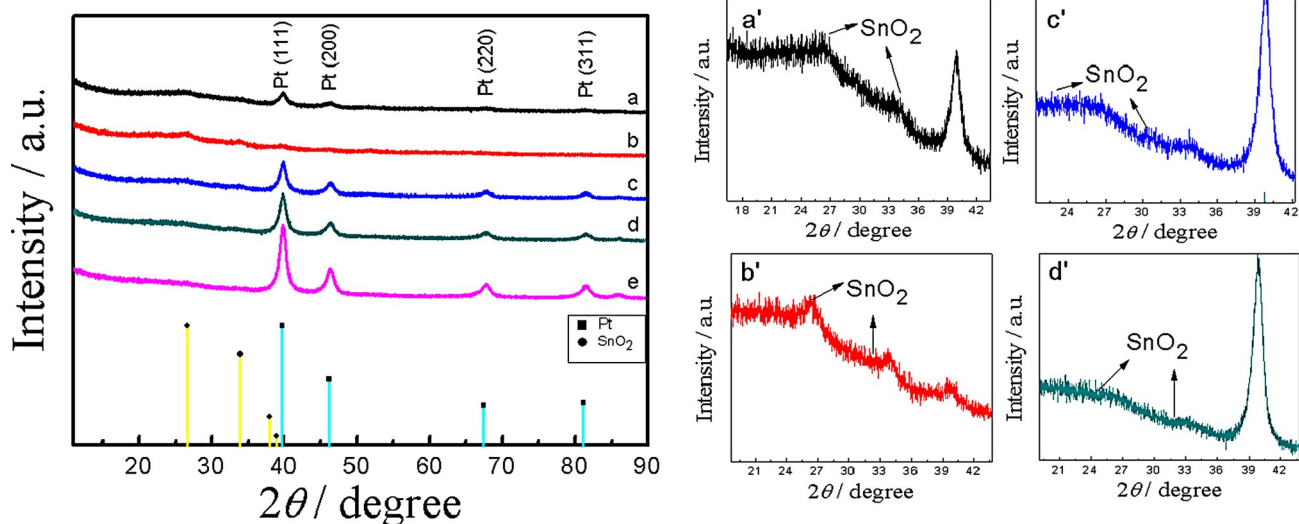


Figure 3. XRD patterns of Pt₁Sn₁ (a), Pt₁Sn₂ (b), Pt₂Sn₁ (c), Pt₃Sn₁ (d) and Pt₅Sn₁ (e). Enlarged patterns of a' (Pt₁Sn₁), b' (Pt₁Sn₂), c' (Pt₂Sn₁), and d' (Pt₃Sn₁).

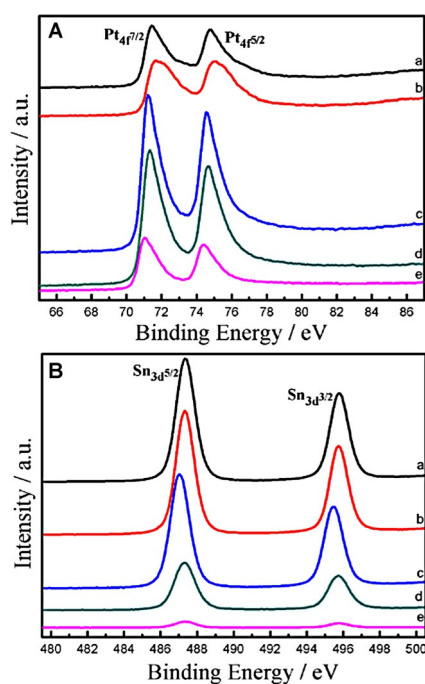


Figure 4. Pt_{4f} and Sn_{3d} XPS spectra of the PtSn catalysts: Pt₁Sn₁ (a), Pt₁Sn₂ (b), Pt₂Sn₁ (c), Pt₃Sn₁ (d), and Pt₅Sn₁ (e).

Table 2. Comparison of binding energies of Pt_{4f}^{7/2} and Sn_{3d}^{5/2} between literature and experiment.

Refs.	Literature data			Experimental data (this study)				
Pt _{4f} ^{7/2}	Pt ⁰	Pt ²⁺	Pt ⁴⁺	Pt ₁ Sn ₁	Pt ₁ Sn ₂	Pt ₂ Sn ₁	Pt ₃ Sn ₁	Pt ₅ Sn ₁
[36]	70.90	73.60	74.5	71.54	71.86	71.29	71.36	71.12
[37]	71.55	72.90	74.5					
[38]	71.40	72.7	74.6					
Sn _{3d} ^{5/2}	Sn ⁰	Sn ^{4+/2+}	–	Pt ₁ Sn ₁	Pt ₁ Sn ₂	Pt ₂ Sn ₁	Pt ₃ Sn ₁	Pt ₅ Sn ₁
[36]	484.60	486.40	–	487.35	487.32	487.04	487.30	487.35
[37]	485.26	486.87	–					
[38]	484.80	486.90	–					

The Sn_{3d} spectra clearly exhibits intense doublets attributable to the 3d^{3/2}(495.5 eV) and 3d^{5/2}(487.3 eV) of Sn^{2+/4+}. In addition, it is difficult to distinguish between Sn^{II} and Sn^{IV} by XPS because their binding energies have very close values.^[39,40] No doublet resulting from metallic Sn (493.2 and 484.8 eV) was observed, thus suggesting that the surface Sn was completely oxidized to oxide tin. Other researchers also found that most tin atoms existed as oxides in PtSn catalysts prepared by different methods.^[41,42]

Typical TEM images of PtSn catalysts and Pt nanoparticles are presented in Figure 5, and where it can be seen that the PtSn nanoparticles are almost spherical. The corresponding particle-size distribution histograms are shown in Figure 6. The average size of PtSn nanoparticles is around 4–5 nm and there is no apparent difference in the shape and average size among these PtSn bimetallic nanoparticles, meanwhile the average size of Pt nanoparticles is about 7 nm. In catalysis, the size of noble metal particles play a key role in achieving reliable catalytic performance and high efficiency.^[43,44] The average size of

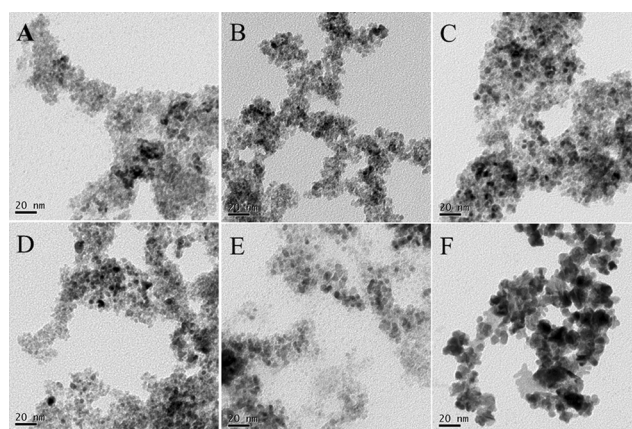


Figure 5. TEM images of Pt₁Sn₁ (A), Pt₁Sn₂ (B), Pt₂Sn₁ (C), Pt₃Sn₁ (D), Pt₅Sn₁ (E), and Pt (F).

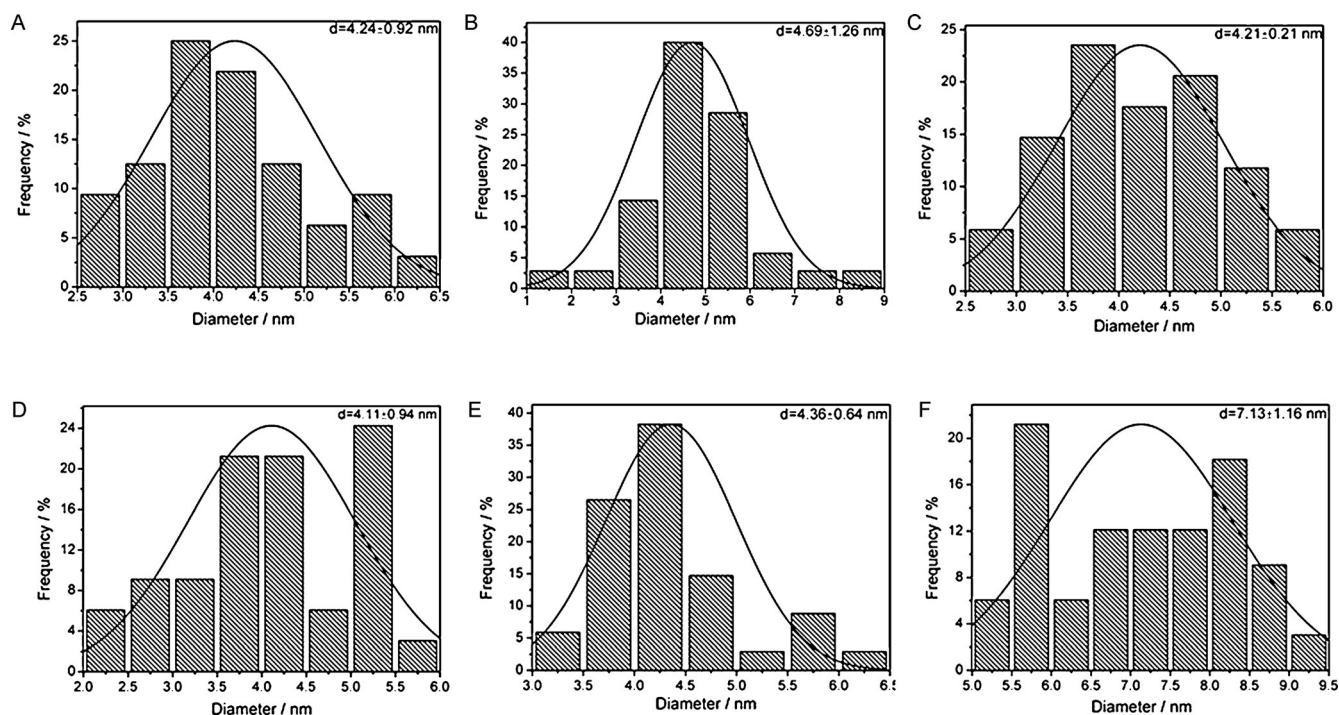


Figure 6. The corresponding particle-size distribution histograms of Pt₁Sn₁ (A), Pt₁Sn₂ (B), Pt₂Sn₁ (C), Pt₃Sn₁ (D), Pt₅Sn₁ (E), and Pt (F).

PtSn nanoparticles is smaller than that of Pt nanoparticles, which suggests that PtSn catalysts have enhanced electrochemical activity compared to Pt.

Electrochemical characterization

Figure 7 shows the cyclic voltammograms of PtSn and Pt catalysts in an alkaline medium. Some typical characteristic regions can be observed in the CV profiles: Hydrogen adsorption/desorption peaks (−1.0 to −0.5 V vs. SCE), electrochemical double-layer region (−0.5 to −0.3 V vs. SCE), peaks for platinum oxide formation (−0.3 to 0.2 V vs. SCE), and platinum oxide reduction regions (−0.5 to 0 V vs. SCE) can be observed

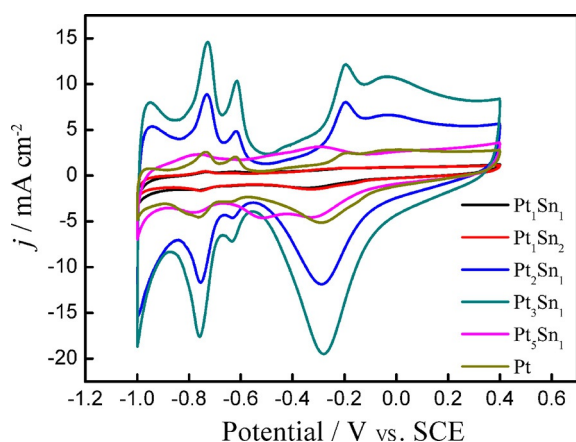


Figure 7. Cyclic voltammograms of Pt₁Sn₁, Pt₁Sn₂, Pt₂Sn₁, Pt₃Sn₁, Pt₅Sn₁, and Pt in 1.0 M KOH solution at a scan rate of 50 mV s⁻¹.

in the image.^[17] In general, Sn pushes hydrogen adsorption/desorption and Pt oxide formation/reduction potentials more negative owing to surface modification. The electrochemically active surface areas (ECSAs) of PtSn/GCE and Pt/GCE have been derived by calculation of hydrogen adsorption/desorption area according to Equation (1):^[45,46]

$$ECSA = \frac{Q_H}{[Pt]0.21} \quad (1)$$

where [Pt] in mg represents the platinum loading in the electrode, Q_H in mC represents the charge that was estimated by hydrogen adsorption/desorption, the constant 0.21 (mC cm⁻²) represents the maximum surface charge transferred to Pt during the adsorption of monolayer of H. The specific calculated value of ECSAs are listed in Table 3. According to a recent report,^[47] a dealloying process occurred in Pt₃Ni₁ catalysts that was beneficial to oxygen reduction reaction (ORR). Based on the results of XRD, it can be assumed that the initial PtSn alloy was followed by dealloying of Sn from Pt and the consequent formation of Pt nanoporous structures, which have indeed been shown to greatly electrocatalytic activity. The discrepancy in ECSA may be explained by the oxidization of Sn, which

Table 3. Comparison of ECSA values (cm² mg⁻¹) for ethanol oxidation on PtSn/GCE and Pt/GCE.

	Pt ₁ Sn ₁	Pt ₁ Sn ₂	Pt ₂ Sn ₁	Pt ₃ Sn ₁	Pt ₅ Sn ₁	Pt
ECSA values	8.71	11.38	173.38	230.82	17.09	37.63

leads to the Sn dealloy from the initial PtSn alloy, thus forming Pt nanoporous structure. As known, the increase of ECSA can promote electrocatalytic activity.^[32, 46]

The catalytic activity of the as-prepared PtSn catalysts was investigated by cyclic voltammetry in a solution of C₂H₅OH (1.0 M)/KOH (1.0 M; Figure 8A). There are two oxidation peaks observed in the voltammograms during the scan: the peak in the forward sweep at about -0.25 V corresponds to the direct oxidation of ethanol, and the other peak in the reverse sweep at about -0.40 V corresponds to the oxidation of intermedi-

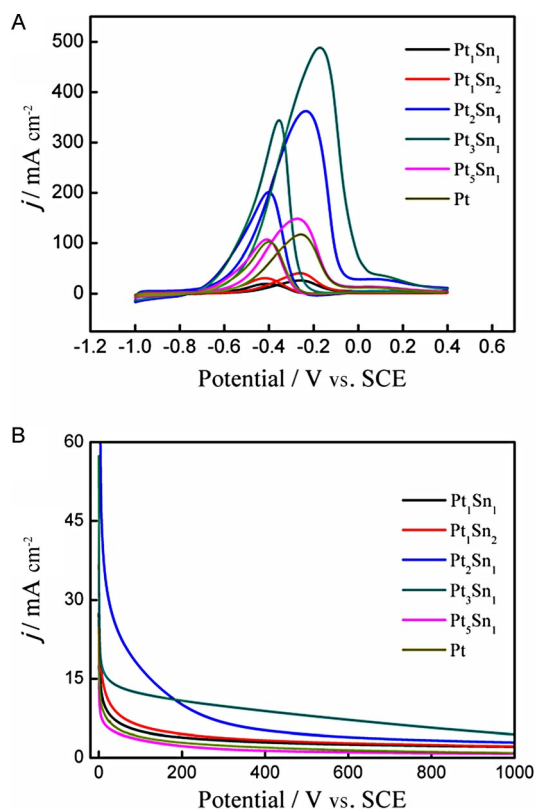


Figure 8. Cyclic voltammograms (A) and chronoamperograms (B) of PtSn/GCE and Pt catalyst in 1.0 M C₂H₅OH/1.0 M KOH solution, respectively. Scan rate: 50 mV s⁻¹.

ates formed in the forward scan.^[48] As seen clearly in Figure 8A, the forward peak-current densities of ethanol oxidation are in the following order: Pt₃Sn₁ > Pt₂Sn₁ > Pt₅Sn₁ > Pt > Pt₁Sn₂ > Pt₁Sn₁. The ECSAs for Pt₁Sn₁/GCE, Pt₁Sn₂/GCE, Pt₂Sn₁/GCE, Pt₃Sn₁/GCE, Pt₅Sn₁/GCE, and Pt/GCE are 8.71, 11.38, 173.38, 230.82, 17.09, 37.63 cm² mg⁻¹, respectively. The integrated areas of the hydrogen absorption and desorption peaks for Pt₃Sn₁ catalysts are larger than other those of PtSn catalysts and Pt catalysts. This outcome suggests that the moderate addition of Sn increases the ECSA of Pt catalysts and enhances the catalytic activity of Pt catalyst toward ethanol electrooxidation.

The long-term stability of different PtSn and Pt catalysts were measured by chronoamperometry in a solution of

C₂H₅OH (1.0 M)/KOH (1.0 M) at -0.25 V (vs. SCE; Figure 8B). For all samples, the current value decreased rapidly in the initial stage, and was probably caused by poisoning of the surface active sites and instability of the catalyst particles.^[49–51] Then the current densities gradually decreased. After 1000 s, the order of the final current densities of these catalysts is: Pt₃Sn₁ > Pt₂Sn₁ > Pt₁Sn₂ > Pt₁Sn₁ > Pt > Pt₅Sn₁. These PtSn catalysts gave higher current density compared with pure Pt, especially Pt₃Sn₁ catalyst, thus demonstrating their greater long-term stability. It confirms that the introduction of Sn can enhance the stability of Pt catalyst towards ethanol electrooxidation. Meanwhile, the Pt₃Sn₁ catalyst presents the highest final current density, which suggests that Pt₃Sn₁ catalyst has the best long-term stability among these PtSn catalysts. Based on the above results, it can be concluded that Pt₃Sn₁ has the highest catalytic performance, thus indicating that the optimum molar ratio of Pt to Sn is 3:1.

Finally, electrochemical impedance spectrometry (EIS) was carried out on Pt₃Sn₁/GCE to evaluate the interfacial processes. Figure 9 shows the Nyquist plots of Pt₃Sn₁/GCE in a solution of C₂H₅OH (1.0 M)/KOH (1.0 M) at different electrode potential from -1.0 to 0.4 V. The ethanol electrooxidation shows different impedance behaviors on PtSn/GCE at various potentials. As seen in Figure 9A, the diameter of the impedance arc (DIA) increases with increasing potentials from -1.0 to -0.5 V. This outcome is possibly due to poisoning and oxidation of the Pt₃Sn₁ catalyst during the reaction. As the potential continuously increases, the arc reverses to the second quadrant at -0.3 V (Figure 9B), and the impedance of the arcs decreases with increase of the electrode potential. This finding is probably due to the reactivation of catalytic active sites, which is related to the removal of reaction intermediates by OH_{ads} adsorbed on the PtSn nanoparticles.^[52] Then the arc gradually flips back to the first quadrant in the potential range from 0 to 0.55 V (Figure 9C), because the surface of the PtSn may be covered by Pt oxides at high potentials, which inhibits the oxidation of ethanol.

Conclusion

Several PtSn composite catalysts with different molar ratio were synthesized by a one-pot chemical reduction method. The composite catalysts display porous structure, and the average size of the nanoparticles are about 4–5 nm. Their electrocatalytic performances towards ethanol electrooxidation in alkaline medium were investigated. According to the results of CV, CA, and EIS, PtSn catalysts present greater catalytic performances toward ethanol oxidation compared with pure Pt catalyst, thus indicating that certain amount of Sn loadings on Pt can enhance the catalytic performance of the Pt catalyst toward ethanol electrooxidation. Meanwhile, results show that Pt₃Sn₁ has the highest catalytic activity, thus demonstrating that a Pt/Sn molar ratio of 3:1 is optimum for the PtSn composite catalyst.

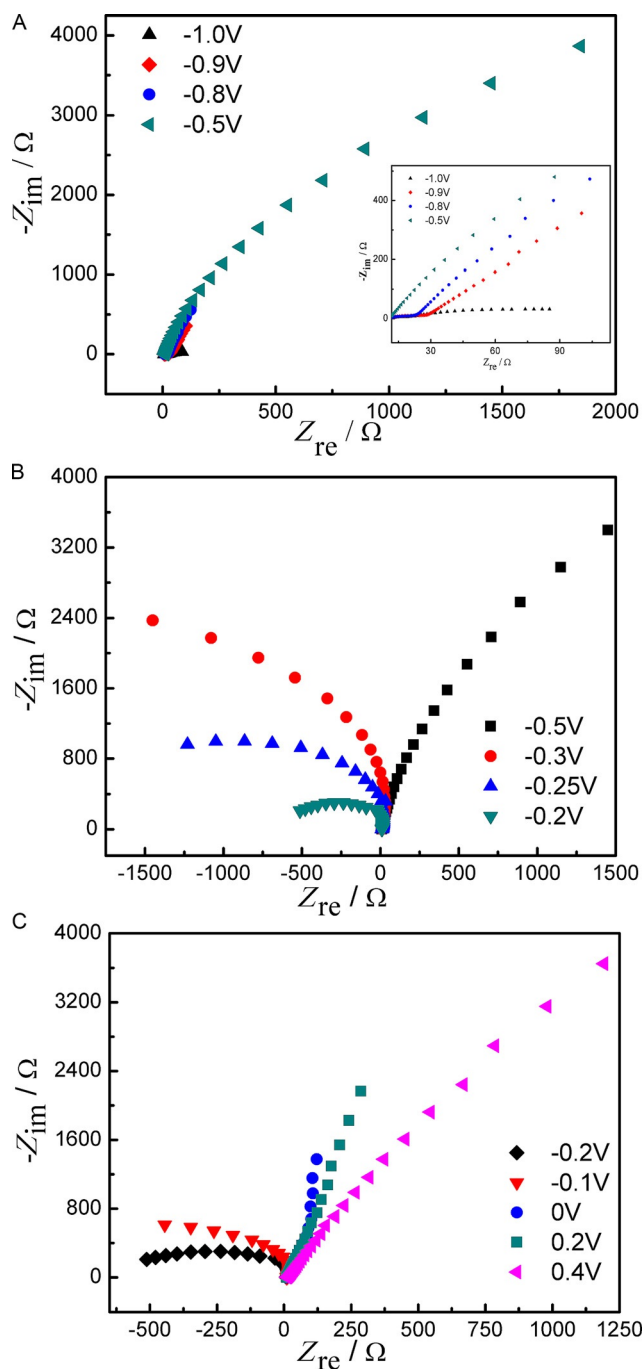


Figure 9. Nyquist plots of ethanol electrooxidation on Pt₃Sn₁/GCE in C₂H₅OH (1.0 M)/KOH (1.0 M) solution at electrode potentials from -1.0 to 0.4 V; inset, magnified region of the Nyquist plots.

Experimental Section

Materials and instruments

H₂PtCl₆·6H₂O, SnCl₂·2H₂O (Shanghai Shiyi Chemicals Reagent Co., Ltd, China), NaBH₄, C₂H₅OH and KOH (Sinopharm Chemical Reagent Co., Ltd, China) were all of analytical grade and used without further purification. Nafion-117 (5 wt%) aqueous solution was purchased from Sigma-Aldrich. Doubly distilled water was used for all the experiments. A scanning electron microscope (SEM, S-4700, Japan) equipped with an energy-dispersive X-ray analyzer (EDX)

was used to determine the morphology and composition of samples. The particle size of all the catalysts was characterized using a TECNAI-G20 electron microscope (TEM) with an accelerating voltage of 200 kV. The crystal structure of the nanomaterials was determined on an X'Pert PRO multiple crystals (powder) X-ray diffractometer (XRD, PANalytical Company, Holland). X-ray photoelectron spectroscopy (XPS) measurements were performed on an ESCALAB220i-XL electron spectrometer from VG Scientific by using 300 W AlK α X-ray radiation for excitation.

All the electrochemical measurements were carried out on a CHI 660B galvanostat (CH Instrumental Co., Ltd., China) with a conventional three-electrode-cell system at room temperature. Pt wire, saturated calomel electrode (SCE), and a GCE (3 mm diameter) were used as the counter, reference and working electrode, respectively.^[45] Cyclic voltammetry (CV) measurement was used to analyze the catalytic activity of as-prepared catalysts in an alkaline media containing C₂H₅OH (1.0 M)/KOH (1.0 M) with a scan rate of 50 mV s⁻¹.

Chronoamperometry (CA) measurements were conducted at -0.25 V in a solution of C₂H₅OH (1.0 M)/KOH (1.0 M) for 1000 s. The electrochemical impedance spectrometry (EIS) was recorded between 1 Hz and 10⁵ Hz with the AC voltage amplitude 5.0 mV.

PtSn electrodes preparation

Please see the Supporting Information for the exact conditions for all catalysts prepared. The appropriate amounts of H₂PtCl₆·6H₂O and SnCl₂·2H₂O were used for obtaining different PtSn molar ratio, such as Pt/Sn = 1:1, 1:2, 2:1, 3:1, and 5:1. A defined amount of SnCl₂ was added to a certain amount of H₂PtCl₆ solution, then fresh aqueous solution of NaBH₄ was added dropwise into the mixture with intense stirring for about 3 h (the amount of NaBH₄ was changed based on the amount of Sn). The suspension was washed, filtered, and dried. Then the as-obtained black powder was dispersed in 2 mL of doubly distilled water with the addition of 5 μ L Nafion solution. After ultrasonic homogenization of the suspension, 10 μ L catalyst ink was added dropwise onto the glassy carbon electrode (GCE), which have been polished with alumina slurries using a polishing cloth.^[3,12] The exact quantities used for preparing each catalyst are presented in the Supporting Information.

For comparison, a solution of NaBH₄ was added dropwise to a solution of H₂PtCl₆ under continuous stirring to prepare pure Pt catalyst. Meanwhile all other steps were the same as for the preparation of PtSn catalysts.

Acknowledgements

This study was supported by the National Natural Science Foundation of China (51373111), the Opening Project of Xinjiang Key Laboratory of Electronic Information Materials and Devices (XJYS0901-2010-01), the Project of Scientific and Technologic Infrastructure of Suzhou (SZS201207), the Suzhou Nano-project (ZXG2012022), the Priority Academic Program Development of Jiangsu Higher Education Institutions (PAPD), and the Academic Award for Young Graduate Scholar of Soochow University.

Keywords: alkaline solutions · ethanol electrooxidation · nanoparticles · platinum · tin

- [1] B. Habibi, S. Ghaderi, *Int. J. Hydrogen Energy* **2015**, *40*, 5115–5125.
- [2] H. Li, G. Sun, L. Cao, L. Jiang, Q. Xin, *Electrochim. Acta* **2007**, *52*, 6622–6629.
- [3] Y. Guo, Y. Zheng, M. Huang, *Electrochim. Acta* **2008**, *53*, 3102–3108.
- [4] S. García-Rodríguez, M. A. Peña, J. L. G. Fierro, S. Rojas, *J. Power Sources* **2010**, *195*, 5564–5572.
- [5] H. Wang, Z. Jusys, R. J. Behm, *J. Phys. Chem. B* **2004**, *108*, 19413–19424.
- [6] T. Yoshitake, Y. Shimakawa, S. Kuroshima, H. Kimura, T. Ichihashi, Y. Kubo, D. Kasuya, K. Takahashi, F. Kokai, M. Yudasaka, S. Iijima, *Physica B* **2002**, *323*, 124–126.
- [7] J. W. Guo, T. S. Zhao, J. Prabhuram, C. W. Wong, *Electrochim. Acta* **2005**, *50*, 1973–1983.
- [8] X. Li, I. M. Hsing, *Electrochim. Acta* **2006**, *51*, 3477–3483.
- [9] R. Wang, S. Liao, S. Ji, *J. Power Sources* **2008**, *180*, 205–208.
- [10] J. Tayal, B. Rawat, S. Basu, *Int. J. Hydrogen Energy* **2012**, *37*, 4597–4605.
- [11] Q. Wang, G. Q. Sun, L. H. Jiang, Q. Xin, S. G. Sun, Y. X. Jiang, S. P. Chen, Z. Jusys, R. J. Behm, *Phys. Chem. Chem. Phys.* **2007**, *9*, 2686–2696.
- [12] J.-B. Raoof, S. R. Hosseini, S. Z. Mousavi-Sani, *Chin. J. Catal.* **2015**, *36*, 216–220.
- [13] B. Habibi, E. Dadashpour, *Int. J. Hydrogen Energy* **2013**, *38*, 5425–5434.
- [14] E. Antolini, E. R. Gonzalez, *Catal. Today* **2011**, *160*, 28–38.
- [15] R. F. B. De Souza, L. S. Parreira, D. C. Rascio, J. C. M. Silva, E. Teixeira-Neto, M. L. Calegaro, E. V. Spinace, A. O. Neto, M. C. Santos, *J. Power Sources* **2010**, *195*, 1589–1593.
- [16] A. Velázquez-Palenzuela, F. Centellas, E. Brillas, J. A. Garrido, C. Arias, R. M. Rodriguez, P.-L. Cabot, *Int. J. Hydrogen Energy* **2013**, *38*, 16418–16426.
- [17] X. Wang, J. Lian, Y. Wang, *Int. J. Hydrogen Energy* **2014**, *39*, 14288–14295.
- [18] J. Corchado-García, C. R. Cabrera, *Electrocatalysis* **2014**, *5*, 402–407.
- [19] C. Coutanceau, S. Brimaud, C. Lamy, J. M. Léger, L. Dubau, S. Rousseau, F. Vigier, *Electrochim. Acta* **2008**, *53*, 6865–6880.
- [20] L. Jiang, A. Hsu, D. Chu, R. Chen, *Int. J. Hydrogen Energy* **2010**, *35*, 365–372.
- [21] C.-T. Hsieh, Y.-S. Chang, A. K. Roy, P.-Y. Yu, K.-M. Yin, *Electrochim. Acta* **2014**, *149*, 278–284.
- [22] K. E. Elkins, T. S. Vedantam, J. P. Liu, H. Zeng, S. Sun, Y. Ding, Z. L. Wang, *Nano Lett.* **2003**, *3*, 1647–1649.
- [23] J. Zeng, J. Y. Lee, W. Zhou, *Appl. Catal. A* **2006**, *308*, 99–104.
- [24] R. Yue, C. Wang, F. Jiang, H. Wang, Y. Du, J. Xu, P. Yang, *Int. J. Hydrogen Energy* **2013**, *38*, 12755–12766.
- [25] B. Habibi, *Int. J. Hydrogen Energy* **2013**, *38*, 5464–5472.
- [26] R. Ojani, J.-B. Raoof, M. Goli, R. Valiollahi, *J. Power Sources* **2014**, *264*, 76–82.
- [27] M. Batzill, D. E. Beck, B. E. Koel, *Surf. Sci.* **2000**, *466*, L821–L826.
- [28] M. Nakamura, R. Imai, N. Otsuka, N. Hoshi, O. Sakata, *J. Phys. Chem. C* **2013**, *117*, 18139–18143.
- [29] V. R. Stamenkovic, B. S. Mun, M. Arenz, K. J. J. Mayrhofer, C. A. Lucass, G. Wang, P. N. Ross, N. M. Markovic, *Nature Mater.* **2007**, *6*, 241–247.
- [30] S. Agnoli, G. Barcaro, A. Barolo, A. Fortunelli, M. Sambì, F. Sedona, M. D. Marino, T. Skala, G. Granozzi, *J. Phys. Chem. C* **2011**, *115*, 14264–14269.
- [31] G. Samjeské, S. Nagamatsu, S. Takao, K. Nagasawa, Y. Imaizumi, O. Sekizawa, T. Yamamoto, Y. Uemura, T. Uruga, Y. Iwasawa, *Phys. Chem. Chem. Phys.* **2013**, *15*, 17208–17218.
- [32] Y. Chen, J. Wang, X. Meng, Y. Zhong, R. Li, X. Sun, S. Ye, S. Knights, *Int. J. Hydrogen Energy* **2011**, *36*, 11085–11092.
- [33] M. Zhu, G. Sun, Q. Xin, *Electrochim. Acta* **2009**, *54*, 1511–1518.
- [34] Y. Wang, S. Song, G. Andreadis, H. Liu, P. Tsiakaras, *J. Power Sources* **2011**, *196*, 4980–4986.
- [35] L. Jiang, G. Sun, S. Sun, J. Liu, S. Tang, H. Li, B. Zhou, Q. Xin, *Electrochim. Acta* **2005**, *50*, 5384–5389.
- [36] A. K. Shukla, A. S. Aricò, K. M. El-Khatib, H. Kim, P. L. Antonucci, V. Antonucci, *Appl. Surf. Sci.* **1999**, *137*, 20.
- [37] W. Zhou, S. Song, W. Li, Z. Zhou, G. Sun, Q. Xin, S. Douvartzides, P. Tsiakaras, *J. Power Sources* **2005**, *140*, 50–58.
- [38] Y. Wang, G. Wu, Y. Wang, X. Wang, *Electrochim. Acta* **2014**, *130*, 135–140.
- [39] G. Li, P. G. Pickup, *J. Power Sources* **2007**, *173*, 121–129.
- [40] C. He, H. R. Kunz, J. M. Fenton, *J. Electrochem. Soc.* **2003**, *150*, A1017–A1024.
- [41] E. M. Crabb, R. Marshall, D. Thompsett, *J. Electrochem. Soc.* **2000**, *147*, 4440–4447.
- [42] G. Neri, C. Milone, S. Galvagno, A. P. J. Pijpers, J. Schwank, *Appl. Catal. A* **2002**, *227*, 105–115.
- [43] L. Bai, H. Zhu, J. S. Thrasher, S. C. Street, *ACS Appl. Mater. Interfaces* **2009**, *1*, 2304–2311.
- [44] D. Bin, F. Ren, Y. Wang, C. Zhai, C. Wang, J. Guo, P. Yang, Y. Du, *Chem. Asian J.* **2015**, *10*, 667–673.
- [45] D. Bin, F. Ren, H. Wang, K. Zhang, B. Yang, C. Zhai, M. Zhu, P. Yang, Y. Du, *RSC Adv.* **2014**, *4*, 39612–39618.
- [46] Z. Yao, R. Yue, C. Zhai, F. Jiang, H. Wang, Y. Du, C. Wang, P. Yang, *Int. J. Hydrogen Energy* **2013**, *38*, 6368–6376.
- [47] A. Fortunelli, W. A. Goddard III, L. Sementa, G. Barcaro, F. R. Negreiros, A. Jaramillo-Botero, *Chem. Sci.* **2015**, *6*, 3915–3925.
- [48] M. Khosravi, M. K. Amini, *Carbon* **2010**, *48*, 3131–3138.
- [49] F. Jiang, Z. Yao, R. Yue, J. Xu, Y. Du, P. Yang, C. Wang, *J. Solid State Electrochem.* **2013**, *17*, 1039–1047.
- [50] F. Ren, H. Wang, C. Zhai, M. Zhu, R. Yue, Y. Du, P. Yang, J. Xu, W. Lu, *ACS Appl. Mater. Interfaces* **2014**, *6*, 3607–3614.
- [51] F. Ren, H. Wang, M. Zhu, W. Lu, P. Yang, Y. Du, *RSC Adv.* **2014**, *4*, 24156.
- [52] W. Zhou, Y. Du, F. Ren, C. Wang, J. Xu, P. Yang, *Int. J. Hydrogen Energy* **2010**, *35*, 3270–3279.

 Manuscript received: July 11, 2015

Accepted Article published: August 6, 2015

Final Article published: August 26, 2015